Renewable Energy 224 (2024) 120108

Contents lists available at ScienceDirect

Renewable Energy

journal homepage: www.elsevier.com/locate/renene

A robust I–V curve correction procedure for degraded photovoltaic modules

Baojie Li [a], Clifford W. Hansen [b], Xin Chen [a], Demba Diallo [c], Anne Migan-Dubois [c], Claude Delpha [d], Anubhav Jain [a,*]

[a] Energy Technologies Area, Lawrence Berkeley National Laboratory, Berkeley, CA, USA
[b] Sandia National Laboratories, Albuquerque, NM, USA
[c] Université Paris-Saclay, CentraleSupélec, CNRS, GeePs, Sorbonne Université, Gif-sur-Yvette, France
[d] Université Paris-Saclay, CentraleSupélec, CNRS, L2S, Gif-sur-Yvette, France

ARTICLE INFO

Keywords:
IV curve
IV curve correction
Photovoltaic
PV module
PV degradation

ABSTRACT

To enable health monitoring and fault diagnosis of PV modules using current-voltage characteristics (I–V curves), it is generally necessary to correct the I–V curves measured under different environmental conditions to the standard condition. The most common correction methods are those from IEC 60891: 2021 standard. However, these methods can introduce significant errors when dealing with degraded PV modules due to the inability to account for changes in resistance. To address this, we propose an improved I–V curve procedure, denoted $P_{dynamic}$, which considers different types of degradation by dynamically deriving the correction coefficients from the measured I–V curves. To evaluate the performance, we simulate I–V curves across a wide range of irradiance and temperature for the healthy and degraded module, where the degradation involves increased series resistance, decreased shunt resistance, or both. The results reveal that $P_{dynamic}$ can produce corrected I–V curves closer to the reference ones than Procedures 1, 2, and 4 of the IEC 60891:2021 standard. Moreover, $P_{dynamic}$ exhibits resilience to both seasonal fluctuations and varying levels of degradation. These results highlight $P_{dynamic}$ as a promising and robust I–V curve correction method, particularly for degraded PV modules. A Python-based open-source tool for this procedure is also available at https://github.com/DuraMAT/IVcorrection.

1. Introduction

Current-voltage characteristics (I–V curves) hold valuable information regarding the health of a photovoltaic (PV) module or array [1,2]. Generally, I–V curves are measured by I–V tracing devices for a PV module or a small-scale PV array [3,4]. In recent years, some hardware solutions, like the integration of measurement units into the PV system inverters [5], have been made available for commercial use to record I–V curves for large-scale arrays or power plants [6]. The implementation of commercial I–V curve tracers may face several challenges, including compromised accuracy due to variable weather conditions, safety concerns related to disconnecting high-voltage devices, and disruptions to the normal operation of PV systems [7]. Despite these challenges, as on-site I–V curve measurements become increasingly available, the health monitoring and fault diagnosis of PV modules using I–V curves have garnered significant research interest [8,9].

Environmental factors such as irradiance and temperature significantly influence the shape of field I–V curves. As a result, I–V curves measured under different environmental conditions are typically not directly comparable. To achieve comparability, it is necessary to correct (or translate) these curves to an identical environmental condition. After the correction, the entire I–V curve or key curve parameters can be used for health monitoring and fault diagnosis purposes [8,10]. To be specific, key parameters such as the open-circuit voltage (V_{OC}), short-circuit current (I_{SC}), voltage at the point of maximum power (V_{MPP}), current (I_{MPP}) and power (P_m) can be obtained from the corrected I–V curve for power loss analysis [11] or fault detection and diagnosis [12–15]. Furthermore, the equivalent series resistance (R_s) or shunt resistance (R_{sh}) can also be extracted for long-term performance and degradation analysis [4,16].

In this regard, any errors introduced by the correction procedure in the corrected I–V curve or the key curve parameters can potentially affect the performance of health monitoring and fault diagnosis. Hence, it is critical to perform accurate I–V curve correction.

Many correction methods have been proposed in the literature. The most common ones are those from the IEC 60891 standard [17,18]. Its

* Corresponding author.
E-mail address: ajain@lbl.gov (A. Jain).

https://doi.org/10.1016/j.renene.2024.120108
Received 26 September 2023; Received in revised form 22 January 2024; Accepted 6 February 2024
Available online 6 February 2024

latest version 3.0 (released in 2019) [17] introduced four correction procedures, namely Procedure 1, 2, 3, and 4. Compared to the previous version 2.0 (published in 2009) [18], Procedure 4 has been newly introduced, which does not rely on pre-determined correction coefficients [19]. Procedure 2 is also revised by incorporating two additional correction coefficients [20]. Procedures 1 and 3 are unchanged. In addition to those in the standard, several modified methods have been suggested by researchers. Golive et al. [21] introduced a modified Procedure 1 (version 2009) that neglects two correction coefficients. Ding et al. [22] presented an improved Procedure 2 (version 2009) based on PV module modeling. Abe et al. [23] improved the calculation of the correction coefficients of Procedure 2 (version 2009) by reducing the number of required I–V curves. Researchers also explored the mechanism of the correction procedures. Dobreava et al. [24] demonstrated that the nature of the translation involves affine transformations of concave functions on convex sets. Duck et al. [25] evaluated the correction performance across different irradiance and module temperature. Similar work is carried out by Po et al. [26], Raina et al. [27], and Tsuno et al. [28]. Hishikawa et al. [29] explored Procedure 3 using wide-range linear extrapolation under different weather conditions, while Padilla et al. [30] tested Procedure 3 for PV modules of different technologies. Paudyal et al. [31] investigated the temperature coefficient from field data for the I–V curve correction, while Golive et al. [32] evaluated the sensitivity of Procedures 1, 2, and 4 to the temperature coefficients. Overall, researchers investigated various aspects of the existing correction methods from IEC 60891 standard, including translation nature, temperature coefficients, and the impact of environmental conditions.

As the primary application of I–V curve correction is for health monitoring and fault diagnosis of PV modules, these original or adapted IEC 60891:2021 correction procedures have been extensively employed in the field for these purposes. Specifically, Procedure 1 (version 2009) is applied for the correction when the PV module is under conditions such as dust soiling [33,34], shading [35,36], or hot spots [37], and is commonly applied for power rating [38]. Degradation analysis is also a major application; for example, Procedure 1 is employed in Refs. [39–41], Procedure 2 in Ref. [42], and Procedure 3 in Ref. [43]. Additionally, Procedure 2 (version 2009) is also used to correct key I–V curve parameters [12]. These corrected parameters could be subsequently used as inputs for different tools [28] such as machine learning techniques [11,29] to classify the different fault types. For example, in Ref. [44], the I–V curves corrected by Procedure 2 are correlated with PV electroluminescence (EL) images to identify defects in PV modules. In Ref. [45], Procedures 1 and 2 are also explored for the estimation of single-diode model parameters.

It is important to note that all these correction procedures are designed for healthy PV modules. Our previous study [46,47] conducted a comprehensive evaluation of both versions of IEC 60891 standards for faulty PV modules. First, the work in Ref. [46] focused on the 2009 version of IEC 60891 [18], specifically enhancing Procedure 2 by considering the temperature effect on the voltage correction. Note that this adapted procedure belongs to the outdated 2009 version. In 2021, with the release of IEC 60891:2021 [17], we investigated these new procedures for handling faults in PV modules, as detailed in Ref. [47]. Our findings revealed that these updated procedures still fail to address faults or degradation in PV modules, and significant distortion and errors could be introduced to the corrected I–V curves, particularly when the module is degraded. The primary reason for the poor performance of these procedures is that their correction coefficients are set constant and do not adapt to the changing health status of the PV modules. In response to this limitation, we introduce an enhanced I–V curve procedure ($P_{dynamic}$) based on the latest version of the IEC 60891 standard in this paper. This procedure calculates the correction coefficients dynamically from the measured I–V curves with no need for additional measurements, effectively accounting for series, shunt resistance degradation, or both.

The contribution of this work is summarized in the following points: 1) An enhanced I–V correction procedure is proposed for both healthy and degraded PV modules, outperforming the IEC 60891:2021 correction procedures; 2) The procedure demonstrates resilience to seasonal fluctuations and varying degrees of degradation; 3) The procedure is validated using field I–V curves; 4) An open-source Python-based tool is developed to implement the procedure.

The remainder of the paper is outlined as follows: Section 2 describes the research methodology, which includes the generation of I–V curves, common and proposed I–V curve correction procedures, and the metrics to quantify the correction errors. Section 3 presents the correction performance, where the impact of environmental factors and degradation severity are addressed. Section 4 presents the preliminary field tests using the proposed correction procedure. A discussion is provided in Section 4, and Section 5 concludes the paper.

2. Methodology

To investigate the performance of I–V curve correction procedures, it is crucial to eliminate the influence of all other sources of uncertainty, particularly measurement errors related to irradiance, temperature, and I–V curves, which could potentially exceed 5% [48]. Consequently, to evaluate the correction performance accurately and comprehensively, the I–V curves to correct in this section are generated through simulations instead of field measurements. Section 2.1 introduces the generation of I–V curves via simulations. Section 2.2 summarizes the correction procedures that are evaluated in this paper. Section 2.3 defines the metrics to assess the correction performance.

2.1. Simulation of I–V curves

To generate the I–V curves under different conditions, a monocrystalline-silicon (mono-Si) PV module (CanadianSolar CS3K-310) is modeled in Matlab Simulink® [49], as shown in Fig. 1. The module parameters are detailed in Table S1 of Supplementary Information (SI). This model can generate I–V curves under specified environmental conditions and for different R_s and R_{sh} degradation severity.

The PV module is modeled based on the single-diode model (SDM) [50] as depicted in Fig. 2, which contains five parameters: the photocurrent (I_{ph}), series resistance (R_s), shunt resistance (R_{sh}), saturation current (I_o), and the diode factor (n). The relationship between the module voltage and current is expressed in Equation (1).

$$I = I_{ph} - I_0\left[\exp\left(\frac{V + IR_s}{nN_skT/q}\right) - 1\right] - \frac{V + IR_s}{R_{sh}} \quad (1)$$

where, N_s is the number of cells of the PV module; k refers to the Boltzmann constant (1.38×10^{-23} J/K) and q is the electron's charge (1.6×10^{-19} C).

It should be noted that the values of these five SDM parameters

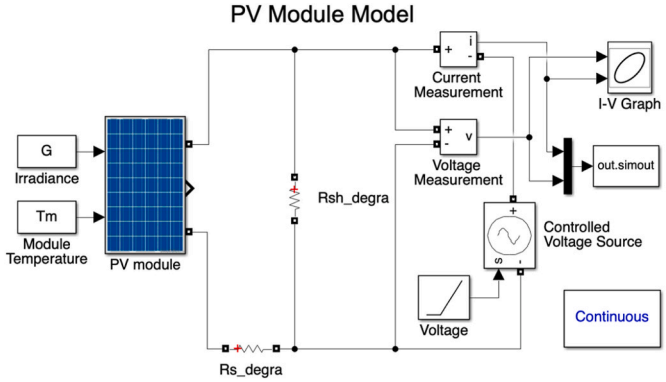

Fig. 1. Simulation model of the PV module under Matlab Simulink.

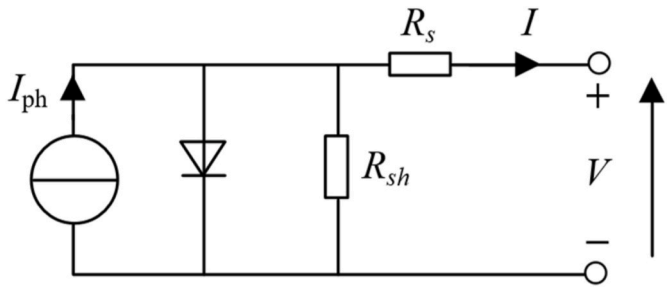

Fig. 2. Single-diode PV cell model.

fluctuate with irradiance and temperature. To transform these parameters from a reference value to a specified irradiance and temperature (generally the Standard Test Condition (STC), irradiance $G = 1000$ W/m^2, module temperature $Tm = 25$ °C), various models [51–53] are available in the literature. The Golive-Model 2 [21] is adopted in this paper. The detailed transformation equations of the five parameters are presented in Section B of the SI.

Based on this PV module model, three conditions are investigated: (i) healthy, (ii) R_s degradation, and (iii) R_{sh} degradation. Specifically, to consider R_s or R_{sh} degradation, an extra resistance R_{s_degra} or R_{sh_degra} is assigned to the PV module, respectively. When the module is in a healthy state, the impact of these additional resistances can be disregarded by setting them to a low (R_{s_degra}) or high (R_{sh_degra}) value, as indicated in Table 1. The variation ranges of R_{s_degra} or R_{sh_degra} are set based on the internal resistances of the PV module. Examples of the I–V curves at STC under the three conditions are displayed in Fig. 3.

2.2. I–V curve correction procedures for evaluation

Our literature review indicates that the most popular I–V curve correction methods are based on the procedures proposed in the IEC 60891 standard. The recent edition 3.0 of the standard (IEC 60891:2021) [17] outlines four procedures (Procedures 1, 2, 3, 4). With pre-determined correction coefficients, Procedures 1, 2, and 4 only need one single measured I–V curve to obtain the I–V curve at the desired condition, whereas Procedure 3 requires at least three measured I–V curves at different irradiance G and module temperature. Procedure 3, due to the difference in the correction nature, is not considered in the following. The new procedure $P_{dynamic}$, proposed in this paper is based on a single I–V curve as Procedures 1, 2, 4. They are outlined below and will be evaluated collectively.

2.2.1. Procedure 1 (P1)

$$I_2 = I_1 + I_{SC1}(G_2/G_1 - 1) + \alpha(T_{m2} - T_{m1}) \tag{2}$$

$$V_2 = V_1 - r_s(I_2 - I_1) - \kappa I_2(T_{m2} - T_{m1}) + \beta(T_{m2} - T_{m1}) \tag{3}$$

where, V_1 and V_2, I_1 and I_2 are the voltage and current before and after correction, respectively. G_1 and T_{m1} refer to the measured irradiance and module temperature, while G_2 and T_{m2} are the target conditions; I_{SC1} is the short-circuit current before correction; α and β are the absolute temperature coefficients of I_{SC} and V_{OC}, respectively, where, $\alpha = \alpha_{rel} \bullet I_{SC}^{STC}$, $\beta = \beta_{rel} \bullet V_{OC}^{STC}$. α_{rel} and β_{rel} are the relative temperature coefficients of I_{SC} and V_{OC}; r_s is the internal series resistance at 25 °C and κ is the curve correction factor. r_s and κ are the pre-determined correction coefficients, which can be calculated using a group of simulated or measured I–V curves at the same G or same Tm [17].

Since STC is generally the preferred condition for I–V curve-based analysis, if not specified otherwise, the I–V curve correction refers to the adjustment to the STC, where $G_2 = 1000 W/m^2$ and $T_{m2} = 25$°C.

2.2.2. Procedure 2 (P2)

$$I_2 = I_1 \frac{G_2}{G_1} \frac{(1 + \alpha_{rel}(T_{m2} - 25))}{(1 + \alpha_{rel}(T_{m1} - 25))} \tag{4}$$

$$V_2 = V_1 - r_{s1}(I_2 - I_1) - \kappa I_2(T_{m2} - T_{m1}) + V_{OC1}\left\{\beta_{rel}[f(G_2)(T_{m2} - 25) - f(G_1)(T_{m1} - 25)] + \frac{1}{f(G_2)} - \frac{1}{f(G_1)}\right\} \tag{5}$$

$$f(G) = B_2 \ln^2(1000/G) + B_1 \ln(1000/\mathrm{G}) + 1 \tag{6}$$

$$r_{s1} = r_s + \kappa(T_{m1} - 25) \tag{7}$$

where, V_{OC1} refers to the open-circuit voltage of the curve before correction; $f(G)$ is a quadratic irradiance-dependent factor accounting for the diode ideality factor. B_1 and B_2 are the irradiance correction factors. r_{s1} is the internal series resistance at the measured T_{m1}. Similar to P1, r_s, κ, B_1, and B_2 are the pre-determined correction coefficients, which are calculated from a group of I–V curves at the same G or same Tm [17].

2.2.3. Procedure 4 (P4)

Procedure 4 is free of the pre-determined correction coefficients (like r_s, κ, B_1, and B_2) required in P1 and P2. Instead, it determines the correction coefficient r_s from the high-voltage region of the measured I–V curve [17].

$$I_1^{'} = I_1 + I_{sc}(G_2 / G_1 - 1)(7) \tag{8}$$

$$V_1^{'} = V_1 - r_s(I_1^{'} - I_1) \tag{9}$$

$$I_2 = I_1^{'} + \alpha_{rel} \times I_{sc}^{STC} \times (T_{m2} - T_{m1}) \tag{10}$$

$$V_2 = V_1^{'} + (T_{m2} - T_{m1})/T_{m1} \times (V_1^{'} - N_s \times \varepsilon) \tag{11}$$

where, ε is a device-dependent constant, representing the product of ideality factor with the bandgap of the photovoltaic material and divided by the electron's elementary charge; The default value of ε is 1.232 V for mono-Si modules [17]; N_s is the number of cells of the module.

For I–V curves measured at low irradiance (<400 W/m^2), the corrected curves using P1 or P4 may not be complete, *i.e.*, part of the I–V curve between maximum power point and V_{OC} point is missing [17]. To obtain complete corrected I–V curves, following the suggestion from the IEC60891:2021 [17], the original I–V curves are extended to make the maximum curve's voltage higher than V_{OC} by either simulation or fitting, with the details provided in Section C of SI.

2.2.4. Proposed procedure ($P_{dynamic}$)

Our previous research has identified that Procedure 2 in the IEC 60891:2021 standard is a promising correction method except under degradation conditions [47]. This is because the correction coefficients do not reflect the PV module's current health condition. To address this issue, we propose a new correction procedure based on Procedure 2. This new procedure introduces two correction coefficients dynamically determined from the I–V curve, considering R_s and R_{sh} degradation. As a result, it can effectively correct the I–V curves for healthy and degraded PV modules. The equations for current and voltage translation are provided in (12-17), while the main differences with Procedure 2 are highlighted in bold. These modifications are deliberately made to ensure

Table 1
Parameter setting for the Healthy, Rs, and Rsh degradation.

Condition	R_{s_degra} (Ω)	R_{sh_degra} (Ω)
Healthy	10^{-5}	10^5
R_s degradation	[10^{-5} – 2]	10^5
R_{sh} degradation	10^{-5}	[15–10^5]

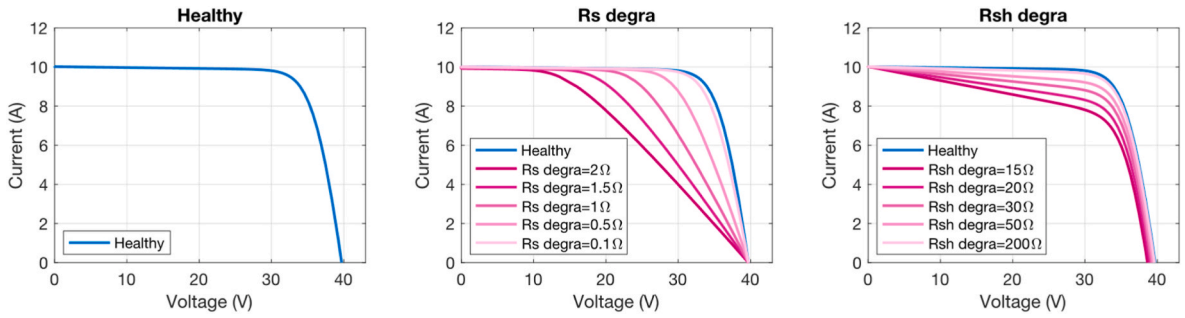

Fig. 3. Examples of I–V curves under Healthy, R_s, and R_{sh} degradation at STC.

the correction procedure can cope with degraded conditions, as explained below.

$$\boldsymbol{I}_1^{'} = \boldsymbol{I}_1 + \boldsymbol{V}_1/\boldsymbol{R}_{sh\_degra} \tag{12}$$

$$\boldsymbol{I}_2^{'} = \boldsymbol{I}_1^{'}\frac{G_2}{G_1}\frac{(1+\alpha_{rel}(T_{m2}-25))}{(1+\alpha_{rel}(T_{m1}-25))} \tag{13}$$

$$\begin{aligned} V_2 = V_1 - R_{s1}\left(\boldsymbol{I}_2^{'} - \boldsymbol{I}_1^{'}\right) - \kappa \boldsymbol{I}_2^{'}(T_{m2}-T_{m1}) \\ + V_{OC1}\left\{\beta_{rel}[f(G_2)(T_{m2}-25) - f(G_1)(T_{m1}-25)] + \frac{1}{f(G_2)} - \frac{1}{f(G_1)}\right\} \end{aligned} \tag{14}$$

$$f(G) = B_2 \ln^2(1000/G) + B_1 \ln(1000/\mathrm{G}) + 1 \tag{15}$$

$$R_{s1} = \boldsymbol{R}_{s\_degra} + \kappa(T_{m1} - 25) \tag{16}$$

$$\boldsymbol{I}_2 = \boldsymbol{I}_2^{'} - \boldsymbol{V}_2/\boldsymbol{R}_{sh\_degra} \tag{17}$$

where, R_s and R_{sh} are the correction coefficients extracted from the I–V curve to correct, reflecting the PV module degradation condition. To be specific, the equivalent circuit of a PV module under R_{sh} degradation can be expressed by connecting an extra resistance R_{sh_degra} in parallel to a healthy module, as illustrated in Fig. 4. Under R_{sh} degradation, if the measured V_1 and I_1 are used as inputs of the original IEC 60891:2021 correction procedures (*e.g.*, P1, P2, P4), the correction performance will be inevitably impacted as these procedures do not consider R_{sh_degra} in their equations. This impact will become more significant when R_{sh_degra} is not negligible. Correction results under this condition will be detailed later in Section 3. Nevertheless, it is worth noting that $I_1^{'}$, the output current of the healthy module, unlike I_1, is not affected by the degradation of R_{sh_degra}, as shown in Fig. 4 (a). Consequently, the pair V_1 and $I_1^{'}$ can be used as inputs of the correction procedures developed for the PV module under healthy conditions.

Specifically, to perform the correction under R_{sh} degradation, the first step is to use the pair $(V_1, I_1^{'})$ (expressed in (12)) is used as input to the correction procedure to obtain corrected V_2 and $I_2^{'}$. Then, the final I_2 is calculated by adding the current affected by R_{sh_degra} as shown in Fig. 4 (b) and expressed in (17).

To consider R_s degradation in the correction, the process is simpler since there is a correction coefficient r_s in the original P2. However, in contrast to r_s in P1 or P2, which is a constant value for I–V curves measured under any environmental condition, in $\mathrm{P_{dynamic}}$, R_{s_degra} is determined from the I–V curve to correct, hence reflecting the degradation effect.

To perform the correction, $\mathrm{P_{dynamic}}$ requires determining the correction coefficients R_{s_degra} and R_{sh_degra} from the measured I–V curve. This paper adopts the Sandia method [54], which is lightweight and has shown reliable performance for various PV technologies (including mono-Si, thin film, and CdTe). Furthermore, after a comprehensive test with varying reference values of R_{s_degra} and R_{sh_degra}, the Sandia method consistently provides accurate estimates of R_{s_degra} and R_{sh_degra} regardless of the variation (detailed in Section D of SI). Therefore, it is selected to determine the dynamic correction coefficients from the measured I–V curve for $\mathrm{P_{dynamic}}$.

To avoid using additional field I–V curves at same G or same Tm as required in P2, the rest coefficients of $\mathrm{P_{dynamic}}$ (κ, B_1, and B_2) are set constant values, which are determined from the I–V curves generated based on the datasheet information.

2.3. Metric for the evaluation of correction performance

To quantify the discrepancy between the corrected and reference I–V curve, the error of area (E_{area}) [55] is computed, as indicated in (18).

$$E_{area} = \left|\frac{A_{error}}{A_{ref}}\right| \times 100\ \% \tag{18}$$

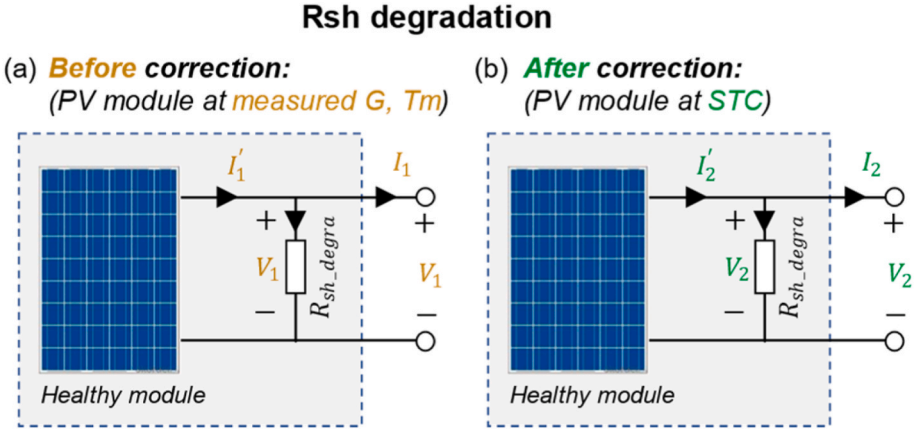

Fig. 4. Equivalent model of PV module under R_{sh} degradation.

Where A_{ref} is the area under the reference curve, and A_{error} the difference between the area under the corrected curve and A_{ref} (directly simulated at STC). An example to illustrate the E_{area} is given in Fig. 5.

3. Correction performance

The I–V curve correction performance can be impacted by the environmental condition (irradiance and temperature) and the degradation severity. Consequently, this section performs an independent evaluation of these factors' effects. Here, we compare the I–V curve correction performance for each method across a wide range of irradiance and temperature conditions, for healthy and degraded modules, where degradation involves increased series resistance, decreased shunt resistance, or both. Section 3.1 explores the effects of G and Tm on the correction performance. Section 3.2 further evaluates the correction performance under realistic environmental conditions based on the four seasons. Section 3.3 investigates the impact of the PV module degradation severity on the correction performance.

3.1. Impact of G and Tm

To examine the influence of G and Tm, G varies from 200 to 1200 W/m^2 in increments of 100 W/m^2 and Tm ranges from 10 to 70 °C in increments of 10 °C. Four module conditions are addressed, healthy, R_s, R_{sh}, and both R_s& R_{sh} degradation. The degradation severities are set with $R_{s\_degra} = 1\ \Omega$ and $R_{sh\_degra} = 20\ \Omega$ for R_s and R_{sh} degradation condition, respectively. These values are determined based on the module internal resistances (presented in Table S2 of SI). The I–V curves generated under these environmental settings and the four module conditions are corrected to STC using P1, P2, P4, and $P_{dynamic}$. The heatmaps of the correction area error are depicted in Figs. 6–10, respectively. The color bar of the heatmap is standardized to ease the comparison. To better illustrate the correction performance, we also display some examples of the corrected curves whose parameters G and Tm are distributed along the diagonal of the heatmap.

3.1.1. PV module under healthy condition

Based on the heatmap, P2 and $P_{dynamic}$ with a lower E_{area}, exhibit similar and better correction performance compared to P1 and P4, especially under low G and high Tm. This is also reflected in the corrected I–V curves shown in Fig. 6(b), where the corrected-to-STC curves match better with the reference one (directly simulated at STC). For a healthy PV module, the coefficient R_{s_degra} used in $P_{dynamic}$ is close to the coefficient r_s in P2 and the impact of coefficient R_{sh_degra} is negligible. Hence, P2 (expressed in (4-7)) and $P_{dynamic}$ (in (12-17)) are almost identical, resulting in comparable correction results.

The impact of G and Tm on the correction E_{area} varies across the procedures. P1 shows greater sensitivity to changes in G, whereas P4 is more strongly influenced by variations in Tm. However, for all procedures, the correction E_{area} tends to decrease as G and Tm are close to STC.

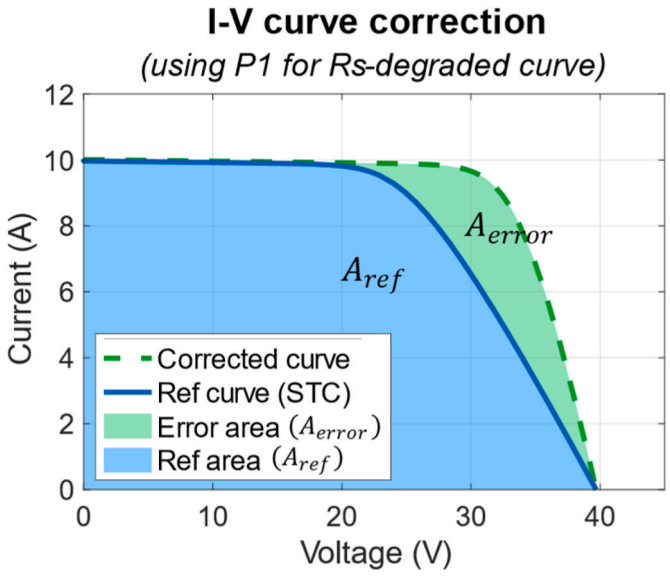

Fig. 5. Illustration of A_{error} and A_{ref} used to calculate E_{area}.

3.1.2. PV module under Rs degradation

Next, we examine the R_s degradation. For P1 and P2, based on the standard [17], the determination of the correction coefficients r_s, κ, B_1, and B_2 requires a group of measured I–V curves at the same G or same Tm. However, this is hard to fulfill in the field, especially for the fixed or operational PV modules [19]. Thus, we investigate two cases here:

- **Case 1**: the groups of degraded I–V curves at the same G or same Tm are *available*. In the simulation, since the extra R_{s_degra} is known (1Ω), we can simulate these two groups of degraded I–V curves to obtain these coefficients for P1 and P2. The corresponding correction results are shown in Fig. 7.
- **Case 2**: the groups of degraded I–V curves at the same G or same Tm are *unavailable*. In this case, the coefficients for P1 and P2 are obtained from the I–V curves generated based on the datasheet information of the PV module. The results are given in Fig. 8.

In Case 1, as depicted in Fig. 7, P1, P2, and $P_{dynamic}$ demonstrate similar excellent performance (mean E_{area} <0.5%). Nonetheless, it is important to highlight that both P1 and P2 require additional I–V curves to determine r_s coefficient. In contrast, both P4 and $P_{dynamic}$ operate without the need for extra measurements. Instead, they dynamically estimate R_s from the measured I–V curve. However, P4 underperforms $P_{dynamic}$ due to the simplified equations where the temperature coefficient β_{rel} are omitted.

As for Case 2, it is observed from Fig. 8 that, in the absence of additional I–V curves to derive r_s coefficient, P1 and P2 can no longer produce the effective correction as in Fig. 7. Instead, they cause significant E_{area} to the corrected I–V curves (E_{area} > 5% and up to 31.7%), particularly around the maximum power point (MPP) region. Furthermore, this distortion becomes more pronounced as G deviates from the STC value (1000 W/m^2).

By comparing the results of Case 1 (Fig. 7) and Case 2 (Fig. 8), it becomes evident that the utilization of P1 and P2 necessitates a trade-off between the accuracy of correction and the complexity of the correction process (including the utilization of additional measurements or lack thereof). In the following simulation evaluations, the scenario with a better performance, i.e., Case 1, is adopted for P1 and P2.

3.1.3. PV module under Rsh degradation

Regarding the R_{sh} degradation, none of the IEC 60891:2021 standard methods perform well. Large correction distortions are observed with P2 near the MPP region, and with P1 and P4 near the short-circuit point. This is due to the absence of a correction coefficient that accounts for R_{sh} in all these procedures. Comparatively, by estimating the actual R_{sh} from the measured I–V curve, and incorporating it into the correction procedure, $P_{dynamic}$ can effectively produce corrected curves that closely match the reference curves, regardless the variations in G and Tm.

3.1.4. PV module under both Rs and Rsh degradation

We further explore the combined degradation of both R_s and R_{sh} degradation. For P1 and P2, the groups of degraded I–V curves at the same G or same Tm are provided by simulation as in Case 1 of Section 3.1.2 for P1 and P2 to extract correction coefficients. Conversely, P4 and $P_{dynamic}$ do not necessitate these extra I–V curves.

When both R_s and R_{sh} degradation occur, the heatmap and the cor-

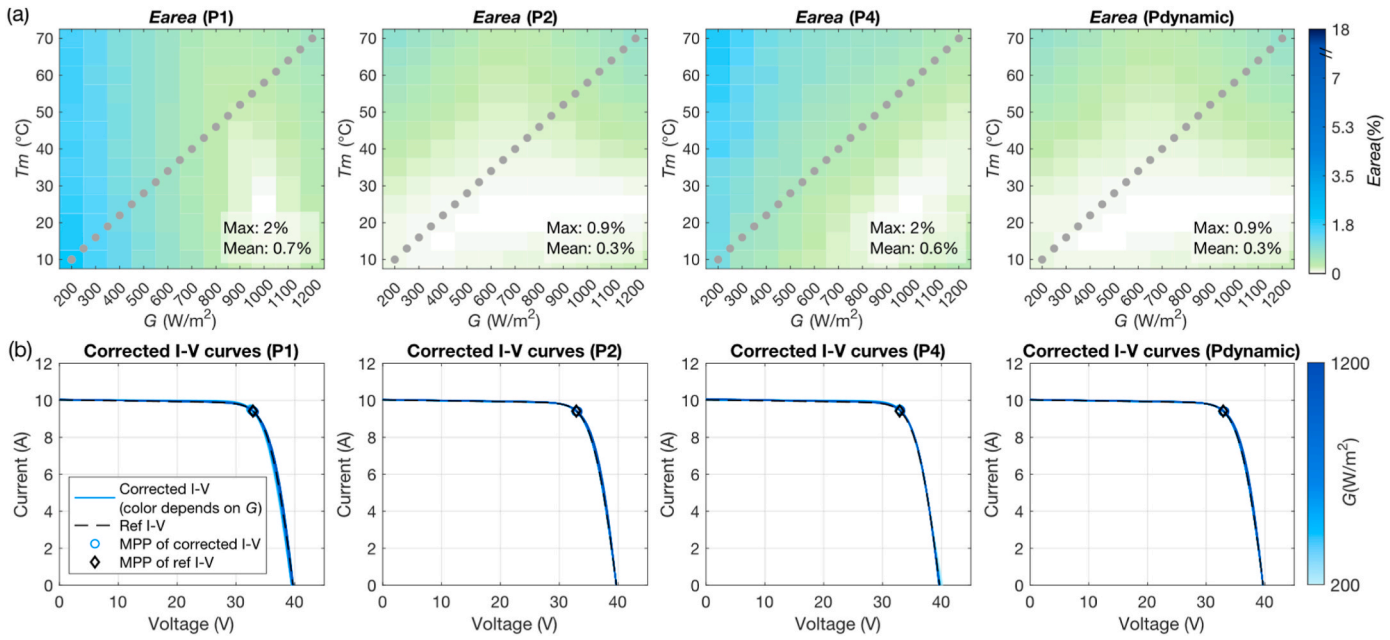

Fig. 6. (a) Heatmap for the area error of the correction of I–V curves under the healthy condition using P1, P2, P4, and $P_{dynamic}$ (gray points represent the *G* and *Tm* of I–V curves shown below); (b) Examples of corrected I–V curves, whose parameters *G* and *Tm* are distributed along the diagonal of the heatmap in (a). It is shown that P2 and $P_{dynamic}$ show overall better correction performance than P1 and P4.(For interpretation of the references to colour in this figure legend, the reader is referred to the Web version of this article.)

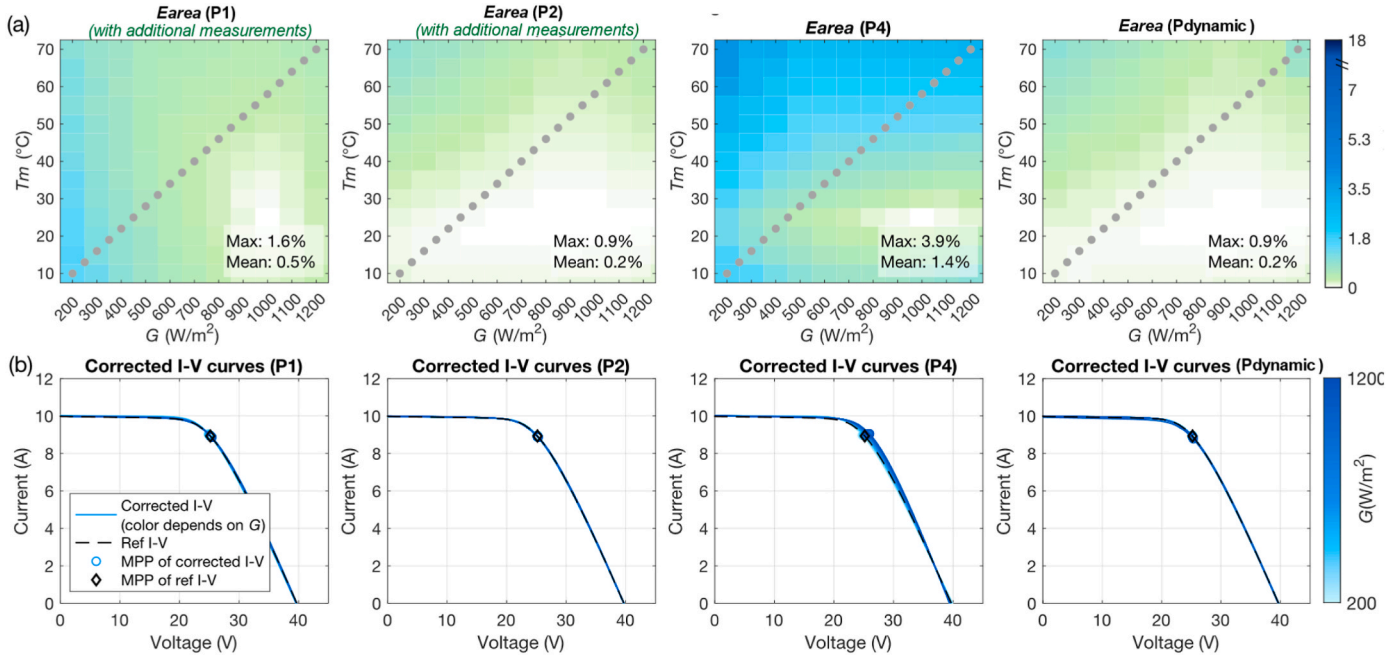

Fig. 7. (a) Heatmap for the area error of the correction of I–V curves under the R_s degradation using P1, P2 (with additional I–V curves), P4, and $P_{dynamic}$ (gray points represent the *G* and *Tm* of I–V curves shown below); (b) Examples of corrected I–V curves whose parameters *G* and *Tm* are distributed along the diagonal of the heatmap in (a). P2 and $P_{dynamic}$ exhibit similar good performance but P1 and P2 require additional I–V curves to obtain r_s coefficient.(For interpretation of the references to colour in this figure legend, the reader is referred to the Web version of this article.)

rected I–V curves exhibit as a combination of the results shown in Figs. 7 and 9. $P_{dynamic}$ still outperforms the other methods even without additional I–V curves as it includes both dynamic correction coefficients (R_{s_degra} and R_{sh_degra}), which effectively reflect the degradation effects.

3.2. Impact of seasons

For field-measured I–V curves, not all the points in the *G-Tm* plane presented in Section 3.1 will be reached in practice. Therefore, to consider the correction performance of the procedures under realistic conditions, the *G* and *Tm* used to generate the I–V curves are determined based on field measurements of one mono-Si PV module in a whole year.

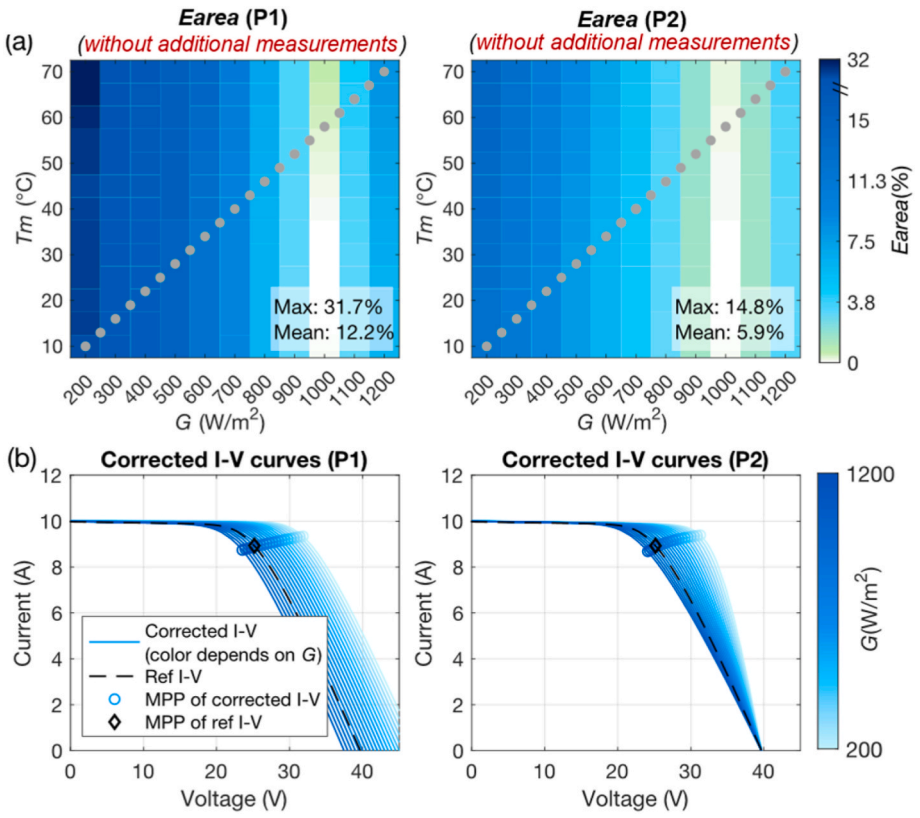

Fig. 8. (a) Heatmap for the area error of the correction of I–V curves under the R_s degradation using P1 and P2 (without additional I–V curves, gray points represent the G and Tm of I–V curves shown below); (b) Examples of corrected I–V curves whose parameters G and Tm are distributed along the diagonal of the heatmap in (a). Without additional I–V curves to obtain r_s coefficient, P1 and P2 could introduce large distortion (E_{area} up to 31.7%) to the corrected curves.(For interpretation of the references to colour in this figure legend, the reader is referred to the Web version of this article.)

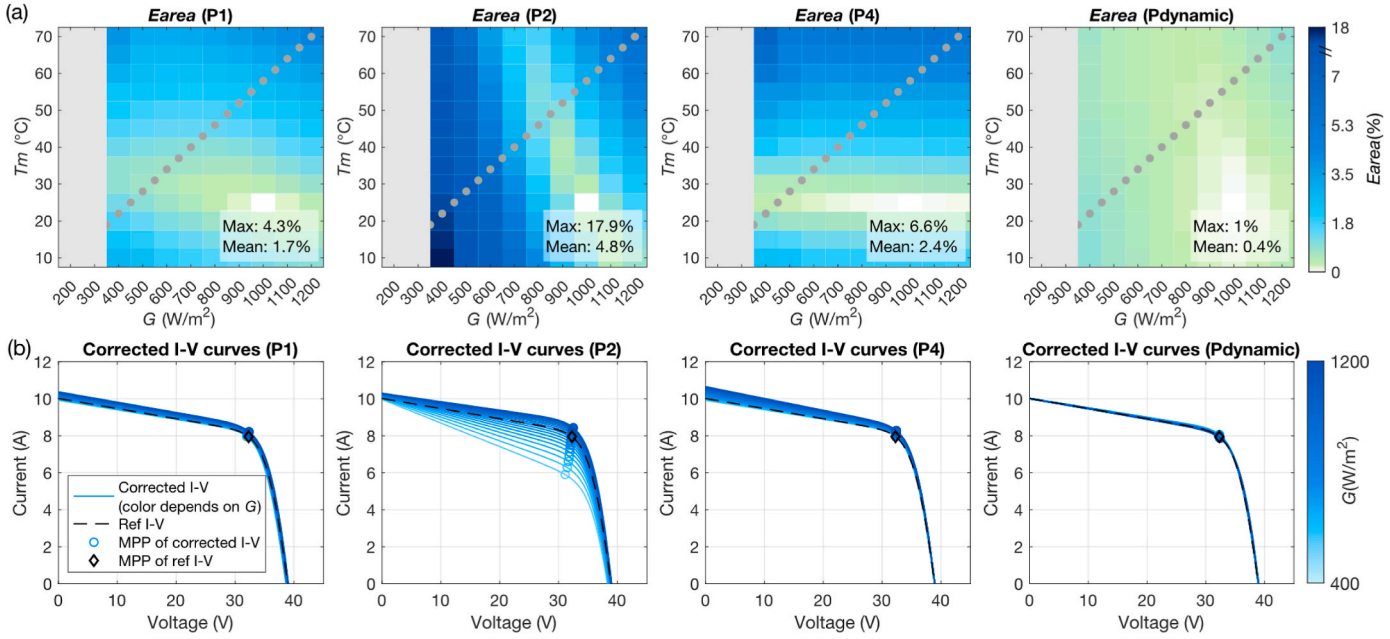

Fig. 9. (a) Heatmap representing E_{area} of the corrected I–V curves under R_{sh} degradation using P1, P2, P4, and $P_{dynamic}$ (gray points represent the G and Tm of I–V curves shown below; results with $G < 400\ W/m^2$ are not displayed due to largely-distorted or invalid correction with examples shown in Section E of SI); (b) Examples of corrected I–V curves, whose parameters G and Tm are distributed along the diagonal of the heatmap in (a). $P_{dynamic}$ clearly outperforms other correction procedures when the module is under R_{sh} degradation.(For interpretation of the references to colour in this figure legend, the reader is referred to the Web version of this article.)

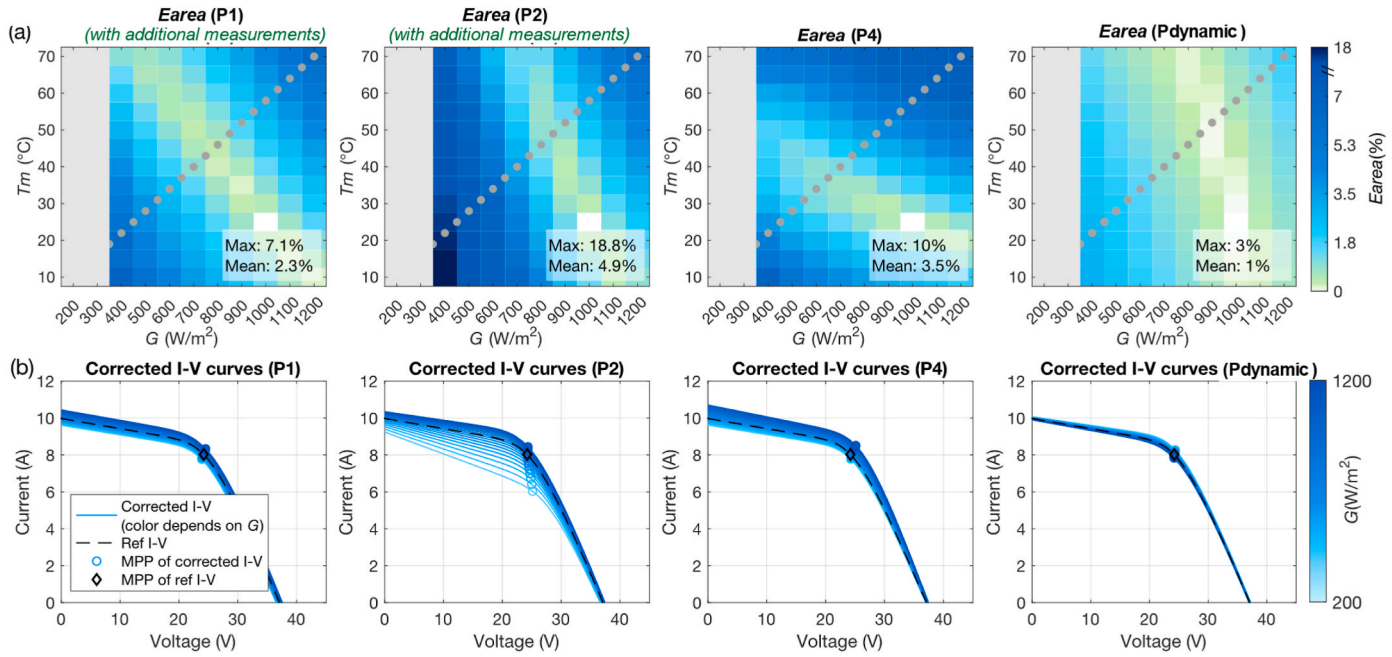

Fig. 10. (a) Heatmap representing E_{area} of the corrected I–V curves under both R_s and R_{sh} degradation using P1, P2 (with additional I–V curves), P4, and $P_{dynamic}$ (gray points represent the G and Tm of I–V curves shown below; results with $G < 400\ W/m^2$ are not displayed due to largely-distorted or invalid correction with examples shown in Section C of SI); (b) Examples of corrected I–V curves, whose parameters G and Tm are distributed along the diagonal of the heatmap in (a). $P_{dynamic}$ still outperforms other correction procedures when both types of degradation are present.(For interpretation of the references to colour in this figure legend, the reader is referred to the Web version of this article.)

The data are split into four seasons, with details are provided in Section F of SI. Using P1, P2, P4, and $P_{dynamic}$, the mean E_{area} of all the corrected curves is presented in Fig. 11 as a function of seasons.

Overall, the E_{area} using the spring and fall I–V curves are similar due to the similar distributions of G and Tm, as presented in Fig. S5. Under the healthy condition, P2, P4, and $P_{dynamic}$ exhibit similar trends with a higher correction error in summer. Conversely for P1, the error is larger in winter. These discrepancies are caused by the difference in G and Tm of the I–V curves across the four seasons (Fig. S5), and the sensitivity of each procedure to G and Tm (as depicted in the heat maps from Figs. 6–10). For example, the E_{area} of $P_{dynamic}$ is more sensitive to Tm. Thus, the correction error gradually decreases from summer to winter. Consistent with the findings in Fig. 6, $P_{dynamic}$ and P2 exhibit similar and better performance compared to P1 and P4 under healthy and R_s degradation. Regarding R_{sh} and combined R_s& R_{sh} degradation, $P_{dynamic}$ outperforms all other methods in all seasons.

Across the four seasons, the average E_{area} is 0.8% for P1, 1.9% for P2, 1.2% for P4, but only 0.27% for $P_{dynamic}$. Note that the excellent performance of $P_{dynamic}$ do not need additional measurements as P1 and P2. This demonstrates the effectiveness of the proposed $P_{dynamic}$ procedure for correcting I–V curves in the presence of faults, and under realistic environmental conditions throughout the year.

3.3. Impact of degradation severity

Sections 3.1 and 3.2 focus on the impact of the environmental parameters with a constant R_s and R_{sh} degradation level. In this subsection, the degradation levels are varied in the following ranges: $[10^{-5}$ - 2] Ω for R_{s_degra} and $[10^5$ - 10] Ω for R_{sh_degra}. The irradiance and temperature module are extracted from the same field measurements as in Section 3.2 to cover all four seasons. Using P1, P2, P4, and $P_{dynamic}$, E_{area}

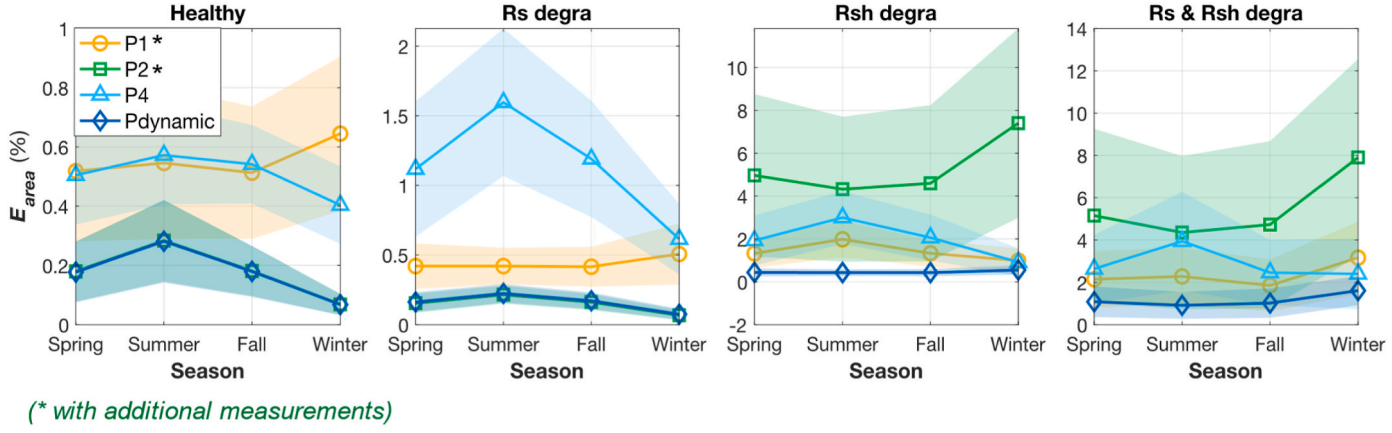

Fig. 11. E_{area} of corrected I–V curves in 4 seasons using P1, P2 (with additional I–V curves), P4, and $P_{dynamic}$ (the dotted line is the mean error in one season while the region refers to the standard deviation). $P_{dynamic}$ exhibits an overall superior correction performance compared to the other procedures. Besides, $P_{dynamic}$ is the least sensitive to the seasonal effects under R_s, R_{sh}, and combined R_s& R_{sh} degradation.

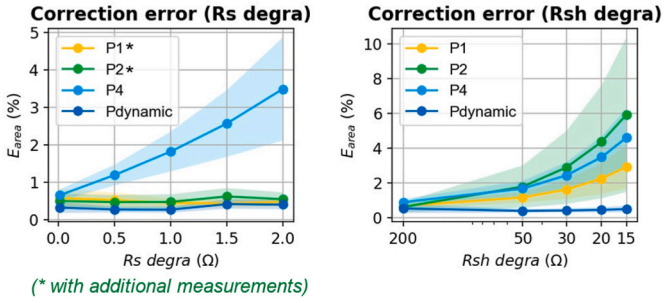

Fig. 12. E_{area} of corrected I–V curves with varying degradation severity. $P_{dynamic}$ is robust to the variation of both types of degradation.

calculated from the corrected curves are presented in Fig. 12 as a function of the degradation severity.

Regarding R_s degradation, it is noted that E_{area} of P4 increases quasi linearly with R_s degradation. While P1, P2 (with additional I–V curves), and $P_{dynamic}$ demonstrate similar and stable performance (E_{area} <1%). As for R_{sh} degradation, all procedures from the IEC standard (P1, P2, and P4) exhibit poor performance, especially with decreasing R_{sh_degra}. In contrast, $P_{dynamic}$ displays excellent and robust correction performance.

In summary, due to the introduction of dynamically determined correction coefficients accounting for the two types of degradation, $P_{dynamic}$ can accurately correct the I–V curves of degraded PV modules without additional measurements even when subjected to variations in the degradation severity.

4. Preliminary field test of correction procedures

The results presented in Section 3 are based on simulated I–V curves. In this section, field-data are used to evaluate the four procedures (the three IEC standard procedures and the proposed $P_{dynamic}$).

4.1. Configuration of in-field I–V curve measurement

The field test bench is located at the SIRTA Atmospheric Research Observatory [56] in Gif-sur-Yvette, France (climate zone T3:H4 based on PVCZ classification [57]), with the configuration illustrated in Fig. 13 (a). A mono-Si type PV module (CanadianSolar CS3K-310) is employed, while a reference cell located in the same plane as the module measures the irradiance. The temperature of the module is recorded using a temperature sensor (Pt100) glued to the backsheet of the module. The I–V curves are measured by connecting the module with a programmable variable load with examples presented in Fig. 13 (b).

4.2. Limits of the field test

It is difficult to make an unbiased assessment of the correction performance of the four procedures using the I–V curves in the field. This is mainly due to two reasons: 1) there is always a measurement uncertainty in the I–V curves, irradiance, and temperature, which could be up to 5% despite routine calibration [48]. In some cases, these uncertainties can exceed the error caused by the correction procedure, such as under healthy conditions. 2) There is a lack of reference curves measured at STC, particularly when the module is configured under different R_s and R_{sh} degradation. Despite these limitations, it is still possible to apply these correction procedures. Indeed, the results will allow a relative comparison of the four procedures.

4.3. Correction results

To demonstrate the I–V curve correction using P1, P2, P4, and $P_{dynamic}$, eighteen I–V curves (*G-Tm* information listed in Table S3) measured under three module conditions are selected: 1) original (here, we no longer name this condition as 'healthy' since the PV module has been in operation for years), 2) R_s degradation (connecting a high-power resistance of 0.5/1/2Ω in series with the module), and 3) R_{sh} degradation (connecting a high-power resistance of 30/50/200 Ω in parallel with the module). The corrected and reference curves are plotted in Fig. 14. Due to the lack of measured curves at STC, the reference curves are generated by simulation (based on the model in Fig. 1) and setting the extra resistances at the same values used in the field.

It should be noted that, for P1 and P2, due to the fixed installation of the module on a tracking rack, we were unable to remove it to record additional I–V curves at constant module temperature or irradiance to determine the correction coefficients. These coefficients are thus obtained from the I–V curves generated based on the datasheet information of the PV module as discussed in Case 2 of Section 3.1.2.

When the module is in its original condition, all four procedures demonstrate effective correction (Fig. 13 (a)) with a mean E_{area} below 1.2%. It may be noticed that these errors are larger than those obtained from the simulation test, for example, the four seasons results in Fig. 11. This is due to the measurement uncertainties, and the unknown health status of the PV module that prevents from generating an accurate reference curve, as explained in Section 4.2.

For R_s degradation (Fig. 13 (b)), when there are no additional I–V curves at constant *G* and *Tm*, consistent with the results observed in the simulated data (Fig. 8), P1 and P2 could introduce significant disparity between the corrected and reference curves. Comparatively, the corrected curves using $P_{dynamic}$ exhibit better agreement as it uses the dynamic coefficient that captures the actual degradation degree. It may be noted that there is still a minor discrepancy between the corrected and reference curves for Pdynamic, suggesting that the PV module has already undergone some degree of R_s degradation after years of in-field operation.

Regarding R_{sh} degradation (Fig. 13 (c)), the corrected curves using P2 and the high-voltage part using P4 exhibit significant mismatch to the

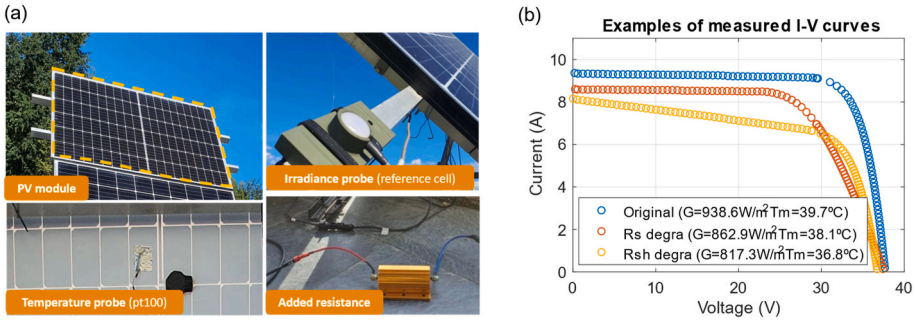

Fig. 13. (a) Configuration of field PV module measurement in SIRTA France. R_s and R_{sh} degradation conditions are set by connecting an additional high-voltage resistance to the module in series or parallel, respectively. (b) Examples of measured I–V curves when the PV module is under original condition, R_s degradation, and R_{sh} degradation.

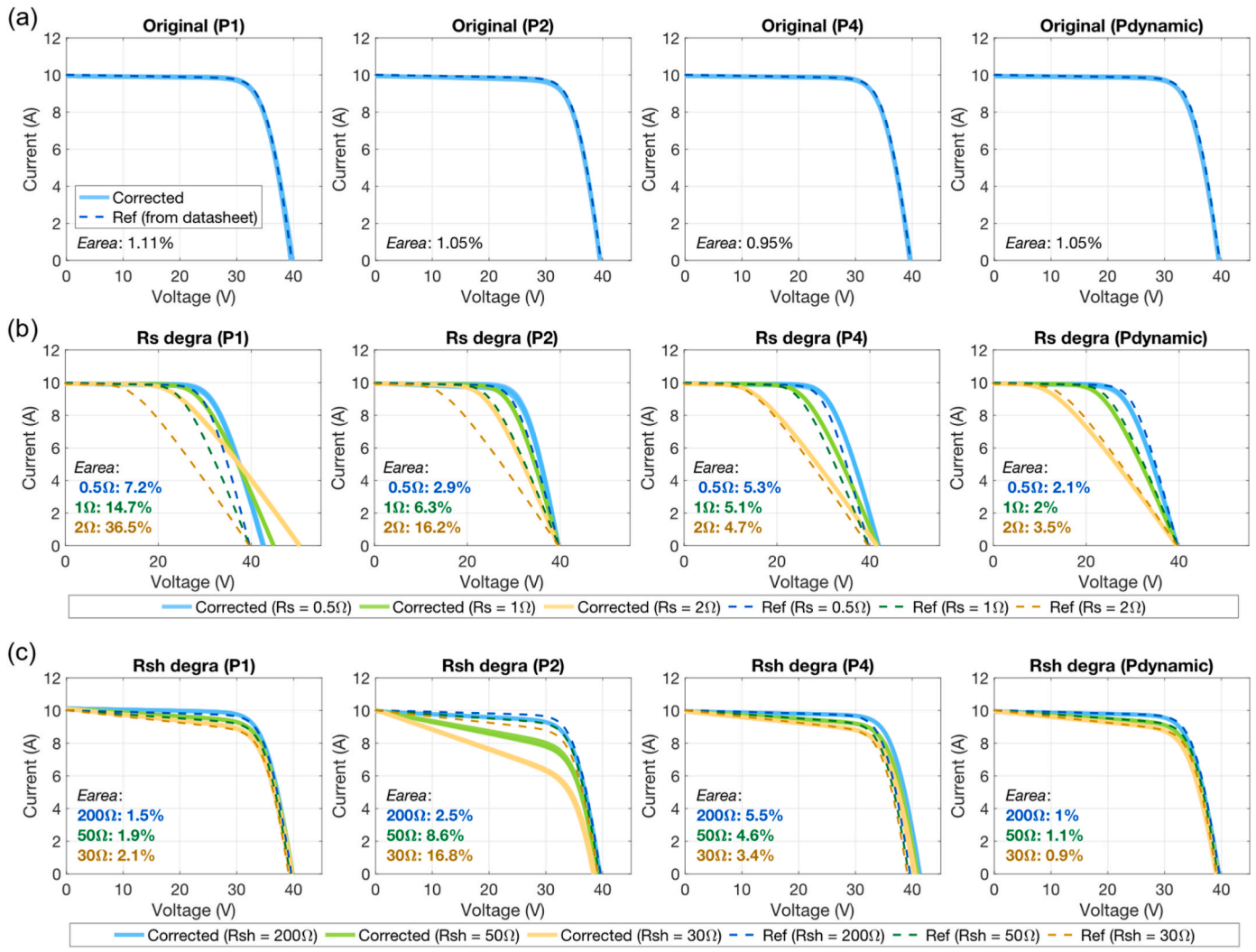

Fig. 14. Corrected field I–V curves under (a) original, (b) R_s degradation, and (c) R_{sh} degradation using P1, P2 (without additional I–V curves), P4, and $P_{dynamic}$. The reference curves are simulated based on the module datasheet information and the additional resistance (for R_s or R_{sh} degradation). It is shown that the corrected curves using $P_{dynamic}$ match better with the reference ones compared to the other procedures, even if the PV module suffers from different degradation levels.

reference curves. P1 and $P_{dynamic}$ achieves similar results with $P_{dynamic}$ showing a lower error. In summary, across both types of degradation scenarios, $P_{dynamic}$ consistently outperforms all other procedures without the use of any additional measurement.

5. Discussion

In IEC 60891:2021 [17], an overview is given on the pros and cons of Procedure 1, 2, and 4 when the PV module is under healthy condition. The major points and the additional findings based on this paper's research (especially when the PV module is degraded and the comparison with the proposed $P_{dynamic}$) are summarized in Table 2.

Alongside its remarkable advantages, the proposed $P_{dynamic}$ procedure also presents certain challenges. Firstly, although the key correction coefficients (R_{s_degra} and R_{sh_degra}) are dynamically determined, the rest ones (κ, B_1, and B_2) are set constant values, which are determined from the I–V curves generated based on the datasheet information. Thus, these coefficients may not fully adapt to field values, particularly for PV modules that have been in operation for several years. Secondly, $P_{dynamic}$ hinges on the Sandia_simple method [54] to extract R_{s_degra} and R_{sh_degra} from the measured I–V curve. However, under certain extreme conditions, such as low G (lower than 300 W/m^2), it may fail to extract the parameters, although such I–V curves are generally unsuitable for assessing the PV module condition.

Despite the challenges, there are also some interesting points to further explore for the I–V curve correction: 1) the determination method of correction coefficients provided in the IEC 60891:2021 standard has strict requirements on G and Tm for measuring the I–V curves, which is hard to fulfill in the field, especially for PV modules in operation. Simplified methods (applicable to field PV modules) to determine these correction coefficients are expected; 2) Regarding the data, all the presented procedures in this paper use a full I–V curve. It is possible to use partially the I–V curve that is of interest for correction [58], such as the region near the maximum power point, open-circuit voltage, or short-circuit current. This would efficiently reduce the time and complexity required to record a full I–V curve; 3) There is a need to investigate the robustness of the correction procedures to the presence of noise in the field-measured I–V data, which may not be as smooth as indoor measurements due to weather fluctuations.

To facilitate the implementation, an open-source Python-based tool for this procedure (https://github.com/DuraMAT/IVcorrection) is developed, with the details presented in Section G of SI.

6. Conclusion

This paper presents a robust I–V curve correction procedure (denoted

Table 2
Pros and Cons of the correction procedures.

	Pros	Cons
P1	• Simple	• Need additional measurement to determine correction coefficient (r_s), otherwise, the performance is affected, especially under R_s degradation • No consideration for R_{sh} degradation • May fail to yield a full corrected I–V curve
P2	• Good performance for healthy PV modules • Produce full corrected I–V curves	• Need additional measurement to determine correction coefficient (r_s), otherwise, the performance is affected, especially under R_s degradation • No consideration for R_{sh} degradation and may cause large distortion
P4	• Free of pre-determined correction coefficients	• Complex procedure to determine correction coefficient (r_s) • May fail to yield a full corrected I–V curve
$P_{dynamic}$	• Best performance under healthy and degradation conditions • Produce full corrected I–V curves • Insensitive to seasons • Robust to varying degradation severity	• Partial correction coefficients (κ, B_1, and B_2) are set constant, which may not adapt to field values • May fail to extract the degradation coefficients (R_{s_degra} and R_{sh_degra}) under low irradiance

as $P_{dynamic}$) suitable for healthy or degraded PV modules. Unlike traditional methods that use constant correction coefficients, $P_{dynamic}$ dynamically derives the coefficients from the measured I–V curves, allowing the actual health status of the PV module to be considered. The results demonstrate that $P_{dynamic}$ outperforms the procedures outlined in the IEC60891:2021 standard, particularly in cases of module degradation, achieving an average correction error of 0.27%, compared to Procedure 1 (1.9%), Procedure 2 (1.2%), and Procedure 4 (0.8%). Furthermore, $P_{dynamic}$ exhibits robustness to the seasonal and degradation severity variations. Preliminary field tests using experimental I–V curves also validated its effectiveness. Finally, an open-source Python-based tool for this procedure is developed. Future works may include improving the robustness of the dynamic coefficient extraction, investigating the impact of measurement uncertainties on the correction performance, and exploring the usage of partial I–V curves for correction.

CRediT authorship contribution statement

Baojie Li: Formal analysis, Methodology, Visualization, Writing – original draft, Writing – review & editing. **Clifford W. Hansen:** Methodology, Writing – review & editing. **Xin Chen:** Methodology. **Demba Diallo:** Methodology, Writing – review & editing. **Anne Migan-Dubois:** Methodology, Writing – review & editing, Writing – original draft. **Claude Delpha:** Conceptualization. **Anubhav Jain:** Funding acquisition, Methodology, Supervision, Writing – original draft, Writing – review & editing.

Declaration of competing interest

The authors declare that they have no known competing financial interests or personal relationships that could have appeared to influence the work reported in this paper.

Acknowledgement

The project was primarily funded and intellectually led as part of the Durable Modules Consortium (DuraMAT), an Energy Materials Network Consortium funded under Agreement 32509 by the U.S. Department of Energy (DOE), Office of Energy Efficiency & Renewable Energy, Solar Energy Technologies Office (EERE, SETO). Lawrence Berkeley National Laboratory is funded by the DOE under award DE-AC02-05CH11231.

Sandia National Laboratories is a multimission laboratory managed and operated by National Technology and Engineering Solutions of Sandia, LLC., a wholly owned subsidiary of Honeywell International, Inc., for the U.S. Department of Energy's National Nuclear Security Administration under contract DE-NA-0003525.

Appendix A. Supplementary data

Supplementary data to this article can be found online at https://doi.org/10.1016/j.renene.2024.120108.

References

[1] K. Zeb, S.U. Islam, I. Khan, W. Uddin, M. Ishfaq, T.D. Curi Busarello, S.M. Muyeen, I. Ahmad, H.J. Kim, Faults and Fault Ride through strategies for grid-connected photovoltaic system: a comprehensive review, Renew. Sustain. Energy Rev. 158 (2022) 112125, https://doi.org/10.1016/J.RSER.2022.112125.
[2] M. Wang, X. Xu, Z. Yan, Online fault diagnosis of PV array considering label errors based on distributionally robust logistic regression, Renew. Energy 203 (2023) 68–80, https://doi.org/10.1016/J.RENENE.2022.11.126.
[3] H. Amiry, M. Benhmida, R. Bendaoud, C. Hajjaj, S. Bounouar, S. Yadir, K. Raïs, M. Sidki, Design and implementation of a photovoltaic I-V curve tracer: solar modules characterization under real operating conditions, Energy Convers. Manag. 169 (2018) 206–216, https://doi.org/10.1016/J.ENCONMAN.2018.05.046.
[4] A. Bouaichi, A. Alami, C. Hajjaj, C. Messaoudi, A. Ghennioui, A. Benlarabi, B. Ikken, A. El, H. Zitouni, In-situ evaluation of the early PV module degradation of various technologies under harsh climatic conditions : the case of Morocco, Renew. Energy 143 (2019) 1500–1518, https://doi.org/10.1016/j.renene.2019.05.091.
[5] S. Spataru, D. Sera, T. Kerekes, R. Teodorescu, Monitoring and fault detection in photovoltaic systems based on inverter measured string I-V curves, in: 31st European Photovoltaic Solar Energy Conference and Exhibition, EU PVSEC), Hamburg, Germany, 2015, pp. 1667–1674, https://doi.org/10.4229/EUPVSEC20152015-5BO.12.2.
[6] Smart I-V Huawei, Curve Diagnosis, 2020. https://solar.huawei.com/en-GB/download?p=%2F-%2Fmedia%2FSolar%2Fattachment%2Fpdf%2Feu%2Fdatasheet%2FIV-Curve.pdf.
[7] S. Sarikh, M. Raoufi, A. Bennouna, A. Benlarabi, B. Ikken, Implementation of a plug and play I-V curve tracer dedicated to characterization and diagnosis of PV modules under real operating conditions, Energy Convers. Manag. 209 (2020), https://doi.org/10.1016/j.enconman.2020.112613.
[8] B. Li, C. Delpha, A. Migan-Dubois, D. Diallo, Fault diagnosis of photovoltaic panels using full I–V characteristics and machine learning techniques, Energy Convers. Manag. 248 (2021) 114785, https://doi.org/10.1016/J.ENCONMAN.2021.114785.
[9] L. Hocine, K.M. Samira, M. Tarek, N. Salah, K. Samia, Automatic detection of faults in a photovoltaic power plant based on the observation of degradation indicators, Renew. Energy 164 (2021) 603–617, https://doi.org/10.1016/J.RENENE.2020.09.094.
[10] A. Mellit, G.M. Tina, S.A. Kalogirou, Fault detection and diagnosis methods for photovoltaic systems: a review, Renew. Sustain. Energy Rev. 91 (2018) 1–17, https://doi.org/10.1016/j.rser.2018.03.062.
[11] M. Wang, J. Liu, T.J. Burleyson, E.J. Schneller, K.O. Davis, R.H. French, J.L. Braid, Analytic I_{sc}–V_{oc} method and power loss modes from outdoor time-series I–V curves, IEEE J. Photovoltaics 10 (2020) 1379–1388, https://doi.org/10.1109/JPHOTOV.2020.2993100.
[12] Z. Chen, L. Wu, S. Cheng, P. Lin, Y. Wu, W. Lin, Intelligent fault diagnosis of photovoltaic arrays based on optimized kernel extreme learning machine and I-V characteristics, Appl. Energy 204 (2017) 912–931, https://doi.org/10.1016/j.apenergy.2017.05.034.
[13] N. Agrawal, B. Bora, A. Kapoor, Experimental investigations of fault tolerance due to shading in photovoltaic modules with different interconnected solar cell networks, Sol. Energy 211 (2020) 1239–1254, https://doi.org/10.1016/j.solener.2020.10.060.
[14] D. Wei, M. Wei, H. Cai, X. Zhang, L. Chen, Parameters extraction method of PV model based on key points of I-V curve, Energy Convers. Manag. 209 (2020) 112656, https://doi.org/10.1016/J.ENCONMAN.2020.112656.
[15] E.D. Chepp, F.P. Gasparin, A. Krenzinger, Improvements in methods for analysis of partially shaded PV modules, Renew. Energy 200 (2022) 900–910, https://doi.org/10.1016/J.RENENE.2022.10.035.
[16] X. Chen, K. Ding, H. Yang, X. Chen, J. Zhang, M. Jiang, R. Gao, Z. Liu, Research on real-time identification method of model parameters for the photovoltaic array, Appl. Energy 342 (2023) 121157, https://doi.org/10.1016/J.APENERGY.2023.121157.
[17] IEC 60891, Photovoltaic Devices - Procedures for Temperature and Irradiance Corrections to Measured I-V Characteristics, 2021.

[18] IEC 60891, Photovoltaic Devices - Procedures for Temperature and Irradiance Corrections to Measured I-V Characteristics, 2009.
[19] Y. Hishikawa, T. Takenouchi, M. Higa, K. Yamagoe, H. Ohshima, M. Yoshita, Translation of solar cell performance for irradiance and temperature from a single I-V curve without advance information of translation parameters, IEEE J. Photovoltaics 9 (2019) 1195–1201, https://doi.org/10.1109/JPHOTOV.2019.2924388.
[20] S. Pingel, D. Erath, T. Wenzel, S. Nold, D. Eberlein, A. De Rose, S. Tepner, J. Schube, G. Ivanov, E. Terukova, A. Moldovan, A. Lorenz, F. Clement, I-V Translation Procedure for Higher Accuracy and Compliance with PERC Cell Technology Requirements, 37th European Photovoltaic Solar Energy Conference and Exhibition, 2020, pp. 1120–1125, https://doi.org/10.4229/EUPVSEC20202020-4AV.2.19.
[21] Y.R. Golive, A. Kottantharayil, J. Vasi, N. Shiradkar, Determining the optimal standard test condition correction procedure for high-throughput field I–V measurements of photovoltaic modules, Prog. Photovoltaics Res. Appl. 30 (2022) 13–26, https://doi.org/10.1002/PIP.3457.
[22] K. Ding, J. Zhang, X. Bian, J. Xu, A simplified model for photovoltaic modules based on improved translation equations, Sol. Energy 101 (2014) 40–52, https://doi.org/10.1016/J.SOLENER.2013.12.016.
[23] C.F. Abe, J.B. Dias, F. Haeberle, G. Notton, G.A. Faggianelli, Simplified approach to adjust IEC-60891 equation coefficients from experimental measurements with long-term validation, IEEE J. Photovoltaics 11 (2021) 496–503, https://doi.org/10.1109/JPHOTOV.2020.3043101.
[24] P. Dobreva, E.E. van Dyk, F.J. Vorster, Irradiance and temperature corrections of current-voltage curves—quintessential nature and implications, Sol. Energy 227 (2021) 116–125, https://doi.org/10.1016/J.SOLENER.2021.08.057.
[25] B.C. Duck, C.J. Fell, B. Marion, K. Emery, Comparing standard translation methods for predicting photovoltaic energy production, Conf. Rec. IEEE Photovolt. Spec. Conf. (2013) 763–768, https://doi.org/10.1109/PVSC.2013.6744261.
[26] S. Haas, A. Bauer, A. Lambertz, U. Rau, Assessment of STC Conversion Methods under Outdoor Test Conditions, 26th European Photovoltaic Solar Energy Conference and Exhibition, 2011, pp. 3458–3462, https://doi.org/10.4229/26THEUPVSEC2011-4AV.1.52.
[27] G. Raina, R. Vijay, S. Sinha, Assessing the suitability of I-V curve translation at varying irradiance and temperature range, Sustain. Energy Technol. Assessments 51 (2022) 101925, https://doi.org/10.1016/J.SETA.2021.101925.
[28] Y. Tsuno, Y. Hishikawa, Comparison of curve correction procedures for current-voltage characteristics of photovoltaic devices, Jpn. J. Appl. Phys. 51 (2012) 10NF02, https://doi.org/10.1143/JJAP.51.10NF02/XML.
[29] S. Wilking, S. Ebert, C. Beckh, A. Herguth, G. Hahn, Precise Determination of the STC I-V Curves by Wide-Range Linear Extrapolation of Outdoor I-V Curves on Partly Sunny Days, 32nd European Photovoltaic Solar Energy Conference and Exhibition, 2016, pp. 1716–1719, https://doi.org/10.4229/EUPVSEC20162016-5DO.11.4.
[30] A. Padilla, C. Londoño, F. Jaramillo, I. Tovar, J.B. Cano, E. Velilla, Photovoltaic performance assess by correcting the I-V curves in outdoor tests, Sol. Energy 237 (2022) 11–18, https://doi.org/10.1016/J.SOLENER.2022.03.064.
[31] B.R. Paudyal, A.G. Imenes, Investigation of temperature coefficients of PV modules through field measured data, Sol. Energy 224 (2021) 425–439, https://doi.org/10.1016/J.SOLENER.2021.06.013.
[32] Y.R. Golive, A. Kottantharayil, N. Shiradkar, Sensitivity of accuracy of various standard test condition correction procedures to the errors in temperature coefficients of c-Si PV modules, in: Progress in Photovoltaics: Research and Applications, 2022, https://doi.org/10.1002/PIP.3559.
[33] J. Tanesab, D. Parlevliet, J. Whale, T. Urmee, T. Pryor, The contribution of dust to performance degradation of PV modules in a temperate climate zone, Sol. Energy 120 (2015) 147–157, https://doi.org/10.1016/j.solener.2015.06.052.
[34] J. Tanesab, D. Parlevliet, J. Whale, T. Urmee, Seasonal effect of dust on the degradation of PV modules performance deployed in different climate areas, Renew. Energy 111 (2017) 105–115, https://doi.org/10.1016/j.renene.2017.03.091.
[35] A. Dolara, G.C. Lazaroiu, S. Leva, G. Manzolini, Experimental investigation of partial shading scenarios on PV (photovoltaic) modules, Energy 55 (2013) 466–475, https://doi.org/10.1016/j.energy.2013.04.009.
[36] S. Fadhel, D. Diallo, C. Delpha, A. Migan, I. Bahri, M. Trabelsi, M.F. Mimouni, Maximum power point analysis for partial shading detection and identification in photovoltaic systems, Energy Convers. Manag. 224 (2020) 113374, https://doi.org/10.1016/j.enconman.2020.113374.
[37] M. Ma, H. Liu, Z. Zhang, P. Yun, F. Liu, Rapid diagnosis of hot spot failure of crystalline silicon PV module based on I-V curve, Microelectron. Reliab. (2019) 100–101, https://doi.org/10.1016/j.microrel.2019.113402.
[38] J.F. Martínez, M. Steiner, M. Wiesenfarth, G. Siefer, S.W. Glunz, F. Dimroth, Power rating procedure of hybrid concentrator/flat-plate photovoltaic bifacial modules, Prog. Photovoltaics Res. Appl. 29 (2021) 614–629, https://doi.org/10.1002/PIP.3410.
[39] F. Martínez-Moreno, G. Figueiredo, E. Lorenzo, In-the-field PID related experiences, Sol. Energy Mater. Sol. Cell. 174 (2018) 485–493, https://doi.org/10.1016/j.solmat.2017.09.037.
[40] M. Piliougine, A. Oukaja, P. Sánchez-Friera, G. Petrone, F.J. Sánchez-Pacheco, G. Spagnuolo, M. Sidrach-de-Cardona, Analysis of the degradation of single-crystalline silicon modules after 21 years of operation, Prog. Photovoltaics Res. Appl. 29 (2021) 907–919, https://doi.org/10.1002/PIP.3409.
[41] N. Kahoul, H. Cheghib, M. Sidrach-de-Cardona, B.C. Affari, M. Younes, Z. Kherici, Performance degradation analysis of crystalline silicon solar cells in desert climates, Energy Sustain. Develop. 65 (2021) 189–193, https://doi.org/10.1016/J.ESD.2021.10.010.
[42] D.A. Quansah, M.S. Adaramola, Ageing and degradation in solar photovoltaic modules installed in northern Ghana, Sol. Energy 173 (2018) 834–847, https://doi.org/10.1016/j.solener.2018.08.021.
[43] M. Piliougine, P. Sánchez-Friera, G. Petrone, F.J. Sánchez-Pacheco, G. Spagnuolo, M. Sidrach-de-Cardona, Analysis of the Degradation of Amorphous Silicon-Based Modules after 11 Years of Exposure by Means of IEC60891:2021 Procedure 3, Progress in Photovoltaics: Research and Applications, 2022, https://doi.org/10.1002/PIP.3567.
[44] V. Kumar, P. Maheshwari, Advanced analytics on IV curves and electroluminescence images of photovoltaic modules using machine learning algorithms, Prog. Photovoltaics Res. Appl. (2021), https://doi.org/10.1002/PIP.3469.
[45] A. Ayang, R. Wamkeue, M. Ouhrouche, M. Saad, T. Andy Tameghe, K. Deli, P. Tchakoua Takoutsing, Least square estimator and IEC-60891 procedure for parameters estimation of single-diode model of photovoltaic generator at standard test conditions (STC), Electr. Eng. 103 (2021) 1253–1264, https://doi.org/10.1007/S00202-020-01131-2/FIGURES/10.
[46] B. Li, A. Migan-Dubois, C. Delpha, D. Diallo, Evaluation and improvement of IEC 60891 correction methods for I-V curves of defective photovoltaic panels, Sol. Energy 216 (2021) 225–237, https://doi.org/10.1016/j.solener.2021.01.010.
[47] B. Li, D. Diallo, A. Migan-Dubois, C. Delpha, Performance evaluation of IEC 60891: 2021 procedures for correcting I–V curves of photovoltaic modules under healthy and faulty conditions, Prog. Photovoltaics Res. Appl. (2022), https://doi.org/10.1002/PIP.3652.
[48] G. Friesen, W. Herrmann, G. Belluardo, B. Herteleer, Report IEA-PVPS T13-11: 2018 Photovoltaic Module Energy Yield Measurements: Existing Approaches and Best Practice, 2018. https://iea-pvps.org/wp-content/uploads/2020/01/Photovoltaic_Module_Energy_Yield_Measurements_Existing_Approaches_and_Best_Practice_by_Task_13.pdf.
[49] The MathWorks Inc, Implement PV Array Modules, The MathWorks Inc., 2023, 2023.
[50] W. De Soto, S.A. Klein, W.A. Beckman, Improvement and validation of a model for photovoltaic array performance, Sol. Energy 80 (2006) 78–88, https://doi.org/10.1016/J.SOLENER.2005.06.010.
[51] R. Singh, M. Sharma, R. Rawat, C. Banerjee, An assessment of series resistance estimation techniques for different silicon based SPV modules, Renew. Sustain. Energy Rev. 98 (2018) 199–216, https://doi.org/10.1016/j.rser.2018.09.020.
[52] A.R. Jordehi, Parameter estimation of solar photovoltaic (PV) cells: a review, Renew. Sustain. Energy Rev. 61 (2016) 354–371, https://doi.org/10.1016/J.RSER.2016.03.049.
[53] R. Venkateswari, N. Rajasekar, Review on parameter estimation techniques of solar photovoltaic systems, Int.Transact.Electrical Energy Syst. 31 (2021) e13113, https://doi.org/10.1002/2050-7038.13113.
[54] C.B. Jones, C.W. Hansen, Single diode parameter extraction from in-field photovoltaic I-V curves on a single board computer, in: Conference Record of the IEEE Photovoltaic Specialists Conference, 2019, pp. 382–387, https://doi.org/10.1109/PVSC40753.2019.8981330.
[55] J.C.H. Phang, D.S.H. Chan, A review of curve fitting error criteria for solar cell I-V characteristics, Sol. Cell. 18 (1986) 1–12, https://doi.org/10.1016/0379-6787(86)90002-5.
[56] A. Migan, T. Mambrini, V. Bourdin, J. Badosa, Deployment of a multi-technology photovoltaic module test bench on the SIRTA meteorological and climate observatory, in: 31st European PV Solar Energy Conference and Exhibition, EU-PVSEC), Hamburg, Germany, 2015. https://www.academia.edu/19033875/Deployment_of_a_multi_technology_photovoltaic_module_test_bench_on_the_SIRTA_meteorological_and_climate_observatory. (Accessed 14 August 2020).
[57] T. Karin, C.B. Jones, A. Jain, Photovoltaic Degradation Climate Zones, Conference Record of the IEEE Photovoltaic Specialists Conference, 2019, pp. 687–694, https://doi.org/10.1109/PVSC40753.2019.8980831.
[58] H. Kalliojärvi, K. Lappalainen, S. Valkealahti, Feasibility of photovoltaic module single-diode model fitting to the current–voltage curves measured in the vicinity of the maximum power point for online condition monitoring purposes, Energies 15 (2022) 9079, https://doi.org/10.3390/EN15239079, 15 (2022) 9079.